



**HAL**  
open science

# Operational Multiple-Doppler Wind Retrieval Inferred from Long-Range Radial Velocity Measurements

Olivier Bousquet, Pierre Tabary, Jacques Parent Du Châtelet

► **To cite this version:**

Olivier Bousquet, Pierre Tabary, Jacques Parent Du Châtelet. Operational Multiple-Doppler Wind Retrieval Inferred from Long-Range Radial Velocity Measurements. *Journal of Applied Meteorology and Climatology*, 2008, 47, pp.2929-2945. 10.1175/2008JAMC1878.1 . meteo-00358754

**HAL Id: meteo-00358754**

**<https://meteofrance.hal.science/meteo-00358754>**

Submitted on 10 Jun 2021

**HAL** is a multi-disciplinary open access archive for the deposit and dissemination of scientific research documents, whether they are published or not. The documents may come from teaching and research institutions in France or abroad, or from public or private research centers.

L'archive ouverte pluridisciplinaire **HAL**, est destinée au dépôt et à la diffusion de documents scientifiques de niveau recherche, publiés ou non, émanant des établissements d'enseignement et de recherche français ou étrangers, des laboratoires publics ou privés.

# Operational Multiple-Doppler Wind Retrieval Inferred from Long-Range Radial Velocity Measurements

OLIVIER BOUSQUET

*CNRM-GAME, Météo-France-CNRS, Toulouse, France*

PIERRE TABARY AND JACQUES PARENT DU CHÂTELET

*Centre de Météorologie Radar, Météo-France, Trappes, France*

(Manuscript received 20 September 2007, in final form 20 February 2008)

## ABSTRACT

The recent deployment of an innovative triple pulse rise time (PRT) scheme within the French operational radar network allows for the simultaneous collection of reflectivity and radial velocity measurements up to a range of 250 km with no ambiguity. This achievement brings new perspectives in terms of operational exploitation of Doppler measurements including the capability to consistently perform multiple-Doppler wind synthesis in a fully operational framework. Using real and simulated Doppler observations, the authors show that the 3D wind fields retrieved in that framework can definitely be relied upon to achieve a consistent and detailed mapping of the airflow structure in various precipitation regimes despite radar baselines averaging  $\sim 180$  km and very limited scanning strategies. This achievement could be easily transposed to other operational networks and represents a remarkable opportunity to add further value to operational Doppler velocity measurements.

## 1. Introduction

Because knowledge of the three-dimensional meso-scale airflow structure presents a significant interest for operational purposes, the ability to perform real-time wind retrieval from operational weather radar has long been a key objective of national weather services operating Doppler radar networks. However, although dual- and multiple-Doppler wind retrieval in precipitation systems has been performed for more than 25 years in research (e.g., Wakimoto and Srivastava 2003), the operational exploitation of Doppler measurements remains generally restricted to single-Doppler analyses, such as Velocity Azimuth Display analysis (VAD; Browning and Wexler 1968), automated short-range detection of wind shifts and microburst in the vicinity of major airports (e.g., Wilson et al. 1984), or ground clutter filtering. The difficulties in achieving operational 3D wind retrieval are primarily related to the “Doppler

dilemma” ensuing from the inverse relationship between the unambiguous range and the unambiguous velocity. This dilemma constrains most operational weather services to restrict their measurements to short range to mitigate velocity ambiguities resulting from the aliasing of radial velocities outside of the Nyquist interval (Doviak and Zrníc 1993). The structure of nearly all operational radar networks being characterized by extensive ( $\sim 200$  km or more) radar baselines, this range limitation negatively impacts the size of the domain where airflow can be successfully reconstructed. Velocity aliasing, which can still significantly impact data quality despite measurement range limitations, slow data transfer, and limited scanning strategies are other important issues that can potentially restrict the operational exploitation of Doppler measurements. For these reasons, real-time (operational) 3D wind synthesis from dual- or multiple-Doppler measurements has never been carried out consistently and has always been limited to field phases during which additional research radars were coupled with operational radars for short periods of time. The first experimentation of this kind was described by Chong et al. (2000), who performed (quasi) real-time dual-Doppler analysis

---

*Corresponding author address:* Dr. Olivier Bousquet, Centre National de Recherches Météorologiques, Météo-France, 42 Avenue G. Coriolis, 31057 Toulouse CEDEX, France.  
E-mail: olivier.bousquet@meteo.fr

of data collected by the French research radar “RONCARD” and Meteo Swiss’s Monte Lema operational radar during the 2-month field phase of the Mesoscale Alpine Programme (MAP). The radar baseline was  $\sim 70$  km long and the method used for synthesizing radial velocities was based on the multiple-Doppler synthesis and continuity adjustment technique (MUSCAT) proposed by Bousquet and Chong (1998). The 3D wind and reflectivity fields reconstructed in this framework were proven quite useful to guide research aircraft in the field, understand the dynamics of the sampled atmospheric systems, or verify numerical model simulations (e.g., Rotunno and Ferretti 2003). More recently, Dolan and Rutledge (2007) also proposed a method to produce real-time dual-Doppler winds as part of a new software suite aiming to assist scientists and forecasters in real-time interpretation and analysis of radar data. The method, which was tested during the summers of 2004 and 2005, was developed for a network of four Doppler radars [two operational Weather Surveillance Radar-1988 Doppler (WSR-88D) and Colorado State University’s (CSU) University of Chicago–Illinois State Water Survey (CHILL) and Pawnee research radars]. Despite the availability of up to four radars simultaneously, it was nevertheless limited to dual-Doppler analysis (with radar baselines ranging from 32 to 80 km), and the operational dual-Doppler pair composed by the two Next Generation Weather Radar (NEXRAD) radars (180-km baseline) was excluded from the analysis.

Thanks to the recent deployment of multiple pulse rise time (PRT) schemes in operational radar systems (Zrníc 1977; Torres et al. 2004; Tabary et al. 2005, 2006), it has become possible to mitigate the long-lasting Doppler dilemma and to achieve extensive Doppler coverage while keeping velocity aliasing at a marginal rate. Together with the ongoing densification of operational radar networks taking place in Europe and the United States (Parent-du-Chatelet et al. 2003; Alberoni et al. 2002; McLaughlin et al. 2005), these achievements open new perspectives in terms of exploitation of operational Doppler velocity measurements, including the ability to routinely perform multiple-Doppler analysis over vast areas from operational weather radar systems. In France, a fully automated analysis was, for instance, recently implemented to achieve three-dimensional wind field retrieval from operational multiple-Doppler observations collected in the greater Paris area. The value of these wind fields in terms of model verification and nowcasting applications has been investigated in Bousquet et al. (2007, 2008), using Doppler data collected during the passage of a

long-lasting frontal precipitation event in northern France.

Although real-time multiple-Doppler analyses shown in Bousquet et al. (2007) were proven quite reliable, authors estimated that further work was needed to assess the performance of the wind retrieval in more complex meteorological situations, as well as to better estimate uncertainties in reconstructed wind fields. The aim of the present paper is thus to complement the analysis of Bousquet et al. (2007) so as to critically evaluate the reliability of these wind fields in other precipitation regimes—including convection—as well as to examine more precisely the difficulties arising from the use of operational radars for multiple-Doppler retrieval. The paper is organized as follows: a brief description of the French operational radar network is given in section 2. The motivations for this work are further described in section 3 together with a description of the experimental setup and data analysis techniques relied upon to produce 3D wind fields in the framework of the French operational radar network. A qualitative evaluation of wind fields retrieved in this framework is performed in section 4 from real-time multiple-Doppler analyses of data collected within a low-level cyclone and a severe squall line. Simulated radar datasets are then relied upon in section 5 to perform a more objective evaluation of retrieved wind fields. The sensitivity of the retrieval to radar density—the baselines of the French radar network average around 180 km—and to typical operational scanning strategies is also investigated so as to determine more precisely the origin of uncertainties in retrieved winds.

## 2. The French operational radar network

The French operational radar network, Application Radar a la Météorologie InfraSynoptique (ARAMIS), was composed in 2002 of 18 conventional, non-Doppler, weather radars used for rain detection and hydrological purposes. Doppler capabilities have been introduced in 2002 following the beginning of a 6-yr-duration upgrade program called *Projet ARAMIS Nouvelles Technologies en Hydrométéorologie Extension et Renouvellement* (PANTHERE), whose objectives are to modernize the network (through implementing Doppler and polarimetric capabilities) and to fill some gaps in the radar coverage (Parent-du-Chatelet et al. 2003). As of today, ARAMIS comprises 24 radars (Fig. 1), among which are 3 dual-polarimetric radars (Gourley et al. 2006) and 12 Doppler radars that are all equipped with the triple PRT Doppler scheme proposed by Tabary et al. (2006). Although the full Dopplerization of the network is not expected until late 2008, the deployment of this innovative Doppler

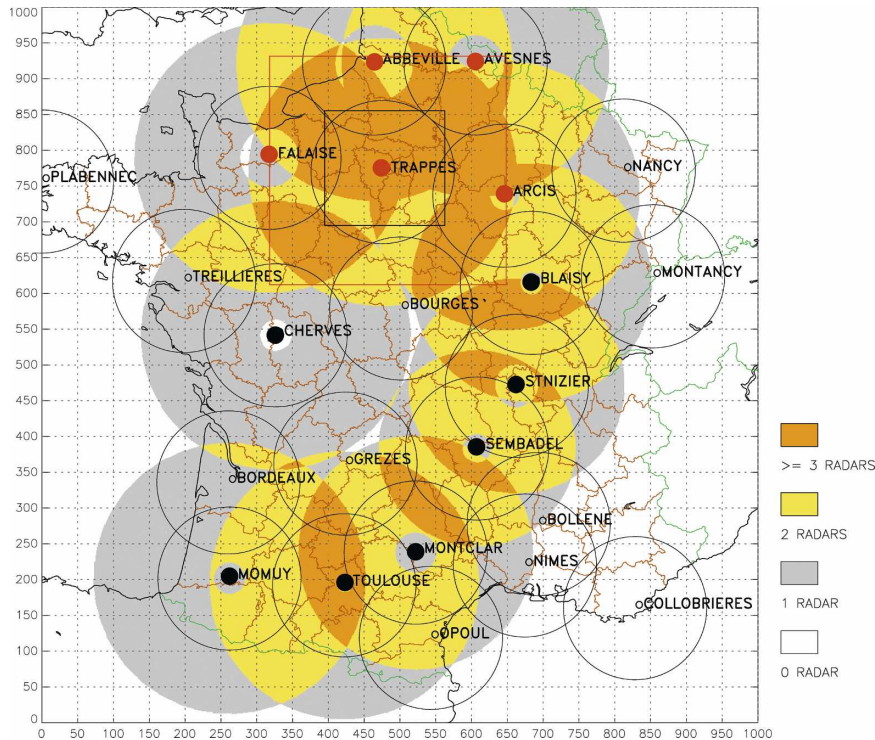


FIG. 1. Map of the French operational radar network ARAMIS. The 100-km ranges of measurement associated with each radar are shown by circles. Doppler radars (as of July 2007) are indicated by red and black dots. Colors indicate regions of single- (gray), dual- (yellow), and multiple-Doppler (orange) coverage at 2500 m MSL. The red (black) square indicates the location of the  $320 \times 320 \text{ km}^2$  ( $160 \times 160 \text{ km}^2$ ) experimental domain used for operational wind retrieval (simulation purposes) using the five radars shown by red dots. The Corsica radar located at Aléria is not shown.

scheme, which yields an extended Nyquist velocity of  $\pm 60 \text{ m s}^{-1}$  up to a range of 250 km, already allows for significant dual- and multiple-Doppler coverage within large portions of the country, especially in northern France and the greater Paris area.

### 3. Operational 3D wind synthesis

#### a. Motivations

A very common way to display radar data is the plan position indicator (PPI) display, which provides a 2D map-like picture of the area covered by the radar beam in which measured heights increase with distance to the radar. Although interpreting PPI displays of scalar fields such as reflectivity is rather intuitive, the physical interpretation of radial velocity PPIs is a time consuming and far more complicated task that requires significant experience and training in radar meteorology. This is illustrated in Fig. 2, which presents low-elevation angle ( $0.4^\circ$ ) PPIs of reflectivity (Fig. 2a) and radial velocity (Fig. 2b) collected by Trappes, France, C-band polarimetric Doppler radar (Fig. 1) during a severe

hailstorm storm that hit Paris on 23 June 2005. At the time of observations (1630 UTC), reflectivity measurements show several spots of intense convective activity resulting from the development of numerous, more or less organized, storm cells up to 60 dBZ within a 100-km range of the radar (Fig. 2a). According to Doppler velocity data (Fig. 2b), the associated airflow was from the east below 0.5 km MSL (that is close to the radar) and from the west above (positive values indicate winds away from the radar), resulting in a vertical wind shear of at least  $10^{-2} \text{ s}^{-1}$  within the 0–1-km layer. Radial velocity measurements also displayed significant spatial variability above 1 km MSL, which suggests that the airflow was fully three-dimensional. Further interpretation of these data is, however, complicated as Doppler velocities only represent a part of the actual wind (i.e., the radial component). These difficulties of interpretation make Doppler radar radial velocity data of little value for the layman. This is particularly true in France where forecasters do not undergo radar training as opposed to, for instance, American or Australian forecasters.

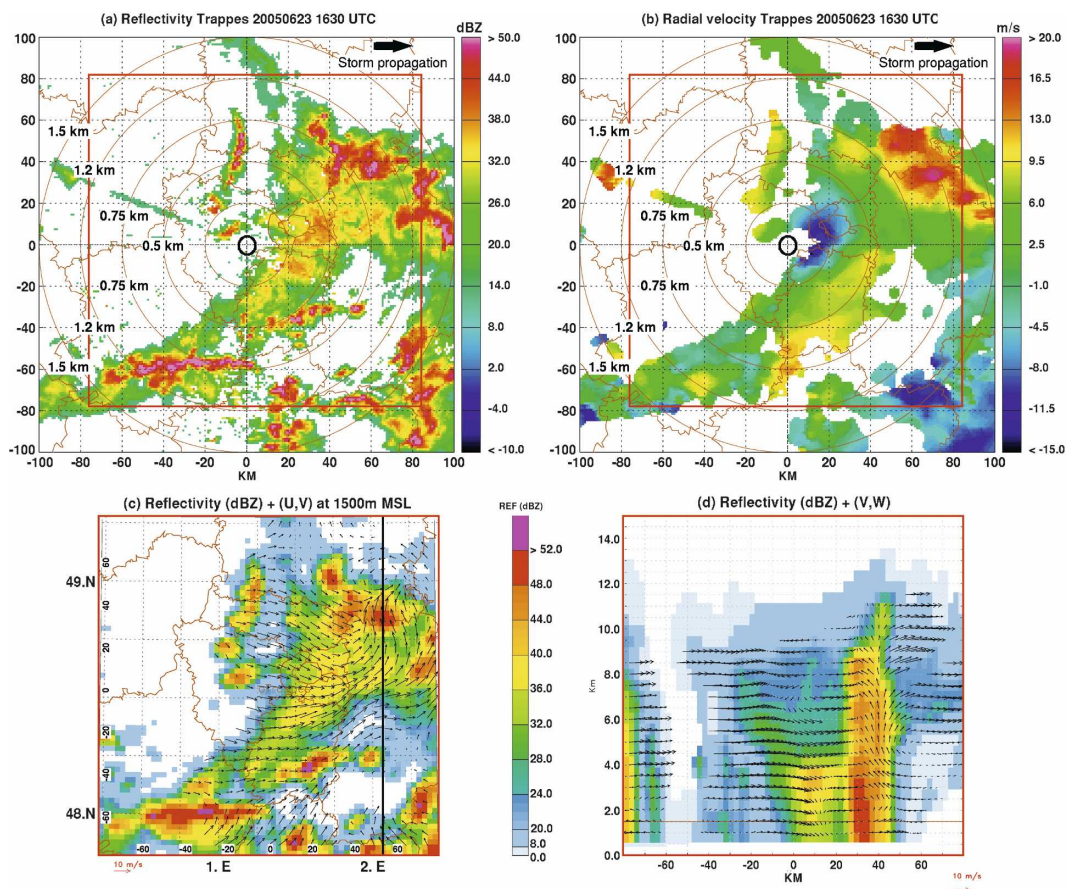


FIG. 2. Radar observations at 1630 UTC 23 Jun 2005. Cartesian, 1-km<sup>2</sup> resolution PPI of (a) reflectivity (dBZ) and (b) radial velocity ( $\text{m s}^{-1}$ ; negative values indicate winds toward the radar) collected by Trappes radar at an elevation of 0.4°. Multiple-Doppler analysis of airflow (vectors) and radar reflectivity (dBZ) within a domain of  $160 \times 160 \times 15 \text{ km}^3$  [shown by red squares in (a) and (b)] centered on Trappes radar with horizontal and vertical resolutions of 2.5 and 0.5 km, respectively. (c) Horizontal cross section at 1.5 km MSL. (d) Vertical cross section along longitude 2.75°E. In (a) and (b), circles indicate the radar range of measurement every 20 km. The height corresponding to each circle is also indicated.

With this background, the main objective of multiple-Doppler analyses, which combine observations collected by several neighboring Doppler radars to reconstruct the 3D wind field within precipitating regions, is to ease the interpretation of airflow and to provide detailed information on the kinematics of observed storms that even a nonradar specialist can easily understand. This capability is illustrated in Figs. 2c,d, which show horizontal wind and reflectivity fields at 1.5 km MSL, as inferred from the synthesis of Trappes, Abbeville, and Arcis radar data (Fig. 1) at the time shown in Figs. 2a,b (the description of the procedures relied upon to produce such 3D wind fields in the framework of the French operational radar network will be provided in the next sections). With respect to the manual analysis of radial velocity data (Fig. 2b), knowledge of the complete wind field evidently allows for a faster and

more comprehensive understanding of the storm kinematical structure. It also provides interesting insights on the storm dynamics through revealing mesoscale wind features that were initially concealed in the radial velocity field, such as a well-defined closed cyclonic circulation at the northern edge of the cloud cluster at  $x = 50 \text{ km}$  and  $y = 50 \text{ km}$  (Fig. 2c).

Another unique benefit of dual- or multiple-Doppler wind synthesis is to provide information on the structure of the vertical motion field. This capability is illustrated in Fig. 2d, which shows a meridional cross section of the airflow and reflectivity field through a deep cell that was observed in the vicinity of the aforementioned mesovortex, ahead of a developing region of stratiform precipitation (see exact location in Fig. 2c). This cell, which exhibited reflectivity values greater than 30 dBZ up to 12-km altitude, was associated with leading up-

TABLE 1. Elevation angles ( $^{\circ}$ ) used in the scanning strategy of the radars covering the greater Paris area. Boldface values correspond to elevations that are used for multiple-Doppler wind retrieval.

Radar/tilt No.	1	2	3	4	5	6	7	8	9	10	11	12	13	14	15	16	17	18
Trappes	90	<b>7.5</b>	0.8	1.5	<b>4.5</b>	0.4	<b>9.5</b>	<b>6.5</b>	0.8	1.5	<b>3.6</b>	0.4	<b>8.5</b>	<b>5.5</b>	<b>0.8</b>	<b>1.5</b>	<b>2.5</b>	<b>0.4</b>
Arcis	<b>4.0</b>	1.1	0.4	—	—	—	<b>3.0</b>	1.1	0.4	—	—	—	<b>2.0</b>	<b>1.1</b>	<b>0.4</b>	—	—	—
Falaise	1.6	1.1	0.4	—	—	—	—	Previous cycle repeated					<b>Previous cycle repeated</b>					
Abbeville	0.4	1.1	0.4	—	—	—	—	Previous cycle repeated					<b>Previous cycle repeated</b>					
Avesnes	1.6	1.0	0.4	—	—	—	—	Previous cycle repeated					<b>Previous cycle repeated</b>					

drafts—on the order of  $5\text{--}6\text{ m s}^{-1}$ —that detrained both southward and northward at top levels to form the cloud anvil. Although the magnitude of these updrafts is likely underestimated with respect to both the vertical extension and the intensity of this particular cell, the retrieved airflow structure seems realistic and is qualitatively consistent with that often observed in multicellular hailstorms from high-resolution research Doppler data (Browning et al. 1976; Houze 1993; Holler et al. 1994). What makes this analysis unique, however, is that it was carried out through synthesizing observations collected by operational radars separated from about 180 km (Fig. 1). Although this work was originally motivated by research purposes in cloud dynamics, the apparent ability to retrieve realistic 3D wind fields from its operational radar network has convinced Météo France to envision the implementation of multiple-Doppler wind retrieval on an operational basis. A prototype allowing real-time synthesis of radial velocity data collected by three radars within a domain of  $160 \times 160 \times 12\text{ km}^3$  (centered on Paris city) was built in June 2006 and later extended to five radars and a domain of  $320 \times 320 \times 12\text{ km}^3$  in November 2006. The procedures used to operationally produce multiple-Doppler analyses from the French radar network are given in the following subsections.

*b. Experimental area*

The main characteristics of the experimental domain are given hereafter, but the reader is referred to Bousquet et al. (2007) for more details about the experimental setup. The current domain of experiment is covered by five C-band Doppler radars located, respectively, at Arcis, Abbeville, and Avesnes, Falaise, and Trappes (Fig. 1). It is centered on Trappes ( $48.77^{\circ}\text{N}$ ,  $2^{\circ}\text{E}$ ,  $\sim 30\text{ km}$  southwest of Paris) and measures  $320\text{ km} \times 320\text{ km} \times 12\text{ km}$ , with horizontal and vertical resolutions of 2.5 and 0.5 km, respectively. All radars perform a complete volume scan in 15 min (supercycle) according to the volume coverage pattern (VCP) demonstrated in Table 1. The scanning strategies are radar specific and have been designed specifically for hydrological purposes. They generally consist of a few low-

elevation scans repeated every 5'. The combination of these limited VCPs with extensive radar baselines (Fig. 1) results in relatively poor radar overlapping in the lowest ( $\leq 1\text{ km}$ ) and highest ( $> 10\text{ km}$ ) layers. The coverage, however, quickly increases with height to reach  $\sim 100\%$  of the domain between 2.5 and 7.5 km. The reader is referred to Bousquet et al. (2007, their Fig. S1) for more details about the radar overlapping within this experimental domain.

*c. Data processing*

Reflectivity and radial velocity observations from the five aforementioned radars are concentrated at the National Center in Toulouse and automatically processed every 15' (radar scans used in the wind synthesis are shown in Table 1). Data consist of Cartesian,  $512\text{ km} \times 512\text{ km}$ ,  $1\text{ km}^2$  in resolution PPIs that are already used for other current operational applications such as VAD analysis, quantitative precipitation estimates, or data assimilation. Spurious reflectivity echoes are eliminated using a threshold on the pulse-to-pulse fluctuation of the reflectivity (following Sugier et al. 2002), and a  $5 \times 5\text{ km}^2$  median filter is applied to radial velocity measurements to filter out potential dealiasing failures (Tabary et al. 2006). Data are then synchronized with respect to the ending time of the 15' period to account for the nonsimultaneity of the measurements. This advection correction is performed through advecting individual bins (pixels) to that common time using a 32-km-resolution, two-dimensional, advection vector field obtained in real time every 5' by cross correlating successive 5' pseudo-constant altitude plan position indicator (pseudo-CAPPI) reflectivity images (as in Tuttle and Foote 1990). Preprocessed data are then interpolated into the Cartesian grid following Cressman (1959) before being ingested in a slightly modified version of the MUSCAT analysis (Bousquet and Chong 1998) that will be presented hereafter. Retrieved wind fields are usually available between 5' and 6' after the completion of a given 15' supercycle: it takes between 3' and 4' to centralize all PPIs in Toulouse (where the main meteorological center is located), about 1 min to preprocess the data, and between 90 and 120 s to syn-

thesize the wind field. As for now, all computations are done on a 1.8-GHz dual-processor Linux server.

*d. The operational version of the MUSCAT formalism*

MUSCAT is a variational algorithm allowing for a simultaneous and computationally efficient solution of the three Cartesian wind components ( $u, v, w$ ) that has been used for more than 10 yr for research applications (e.g., Bousquet and Chong 2000; Pradier et al. 2002; Bousquet and Smull 2006; among others). It was initially proposed by Bousquet and Chong (1998) to eliminate the main drawbacks of iterative techniques commonly employed in dual-Doppler analysis of airborne radar observations before being later extended to ground-based radar measurements (Chong et al. 2000; Chong and Bousquet 2001). Overall, MUSCAT consists of a global minimization, in a least squares sense, of the function  $F$ :

$$F(u, v, w) = \int_S [A(u, v, w) + B(u, v, w) + C(u, v, w)] dx dy, \quad (1)$$

such that

$$\frac{\partial F}{\partial u} \approx 0, \quad \frac{\partial F}{\partial v} \approx 0 \quad \text{and} \quad \frac{\partial F}{\partial w} \approx 0, \quad (2)$$

where  $A$  represents the optimal least squares fit of the observed radial Doppler velocities to the derived wind component. It includes a Cressman distance-dependent weighting function to account for noncollocated data and gridpoint values, allowing the interpolation of the radar data onto the Cartesian grid of interest, in the data fit. In the current framework, the interpolation is performed using a fixed horizontal influence radius of the Cressman weighting function  $R_H$  of 3 km and a variable vertical radius of influence  $R_V$  equal to  $1^\circ$  (beamwidth of the ARAMIS radars). In this configuration,  $R_V$  varies as a function of range so that the search for data points extends farther out at long range compared to short range. This also allows one to indirectly take into account the loss of resolution resulting from beam broadening at long range.

Here,  $B$  is the least squares adjustment with respect to mass continuity. This cost function is formulated for each individual grid box in terms of mass flux throughout the faces of the considered box, which allows one to solve the wind field over both flat and complex terrains (Chong and Cosma 2000). In this formulation the estimated wind components at the previously investigated plane are used as input values to solve for the wind at

the current level. To initialize the wind synthesis, horizontal components are assumed constant between the surface and the first plane for which the solution for the wind components is searched.

Additionally,  $C$  is a constraint allowing one to minimize small-scale wind variations; it is realized through the minimization of the second- and third-order derivatives, which act as low-pass filters. It is controlled by a weighting factor, which is a function of the cutoff wavelength of the filter. In addition to providing more regular fields, this term is also essential to obtaining an objective solution in regions of ill-conditioned analysis through realizing a regular extrapolation in these regions from surrounding properly conditioned areas.

According to previous studies (Lhermitte and Miller 1970; Davies-Jones 1979), the error variances of the horizontal velocity components  $\sigma_u^2$  and  $\sigma_v^2$  inferred from a dual-Doppler radar analysis are related to the Doppler mean velocity variance  $\sigma_r^2$  following

$$\sigma_u^2 + \sigma_v^2 = \frac{2\sigma_r^2}{\sin^2\beta_m}, \quad (3)$$

where  $\beta_m$  defines the angle between the horizontal projection of the two radar beam axes. From Eq. (3), one can define the dual-Doppler coverage area as the locus of points between beam angles  $\beta_{m0}$  and  $\pi - \beta_{m0}$ , where  $\beta_{m0}$  is chosen depending on the maximum tolerated error variance [experimenters usually tolerate an error variance of  $3 \text{ m s}^{-1}$  in the horizontal wind field, which corresponds to an intersecting angle limit ranging between  $20^\circ$  and  $160^\circ$  (Friedrich and Hagen 2004)]. Conversely, all points falling outside this interval define the region of ill-conditioned analysis that is the area where the precision of the reconstructed wind field is problematic. These problems are particularly severe close to the radar baseline (when  $\beta_m$  approaches 0 or  $\pi$ ) and concern more particularly the component of the wind that is normal to this baseline (Miller and Strauch 1974). Although the constraint on second- and third-order derivatives of MUSCAT was initially designed to solve this problem, we found that this low-pass filter could sometimes fail in an operational framework such as ARAMIS, which is characterized by radar separation distances of  $\sim 180 \text{ km}$  (when more than two radars are considered, the actual regions of ill-conditioned analysis fluctuate with height and are functions of radar separation distances and scanning strategies). To mitigate potential errors on cross-baseline wind components in regions of dual-Doppler coverage, a modification of the initial MUSCAT formalism was needed to apply this algorithm in an operational framework without data loss. This change consists of the addition of a

new constraint that allows minimizing the variation of the cross-baseline component of the wind. It is similar to that proposed by Chong and Bousquet (2001) for a dual-Doppler radar network, but is now generalized to a larger number of radars. This term, which only applies in regions covered by two radars, is defined as

$$D = \mu \left( \frac{\partial v'}{\partial y'} \right)^2, \tag{4}$$

where  $v'$  represents the component of the wind along direction  $y'$  in a Cartesian coordinate system  $(x', y', z)$  where  $x'$  coincides with the radar baseline. The weight  $\mu$  is given by

$$\mu = \cos^4 \beta_m. \tag{5}$$

The effect of the constraint is thus maximally close to the radar baseline and weak in properly conditioned areas.

In the original Cartesian coordinate system  $(x, y, z)$ , the operational version of MUSCAT in a generalized form can thus be rewritten as

$$F(u, v, w) = \int_S [A(u, v, w) + B(u, v, w) + C(u, v, w) + D(u, v)] dx dy \tag{6}$$

with

$$D(u, v) = \mu \left[ \frac{\partial(u \sin^2 \alpha_i - v \sin \alpha_i \cos \alpha_i)^2}{\partial x} + \frac{\partial(-u \sin \alpha_i \cos \alpha_i + v \cos^2 \alpha_i)^2}{\partial y} \right], \tag{7}$$

where  $\alpha_i$  is the angle between a given radar baseline and  $x$  axis at grid point  $i$ .

Finally, as the three-dimensional wind field reconstructed by MUSCAT represents a least squares fit to the available observations and does not perfectly satisfy the mass continuity equation, an a posteriori upward integration is needed to refine the first estimation of the vertical velocity. In a research mode this integration is generally performed following the variational approaches proposed by Georgis et al. (2000) or Chong and Testud (1983), which are particularly efficient. These algorithms are nevertheless time consuming and, as such, not really suitable for real-time operational purposes. For this particular application, we thus chose to follow a much simpler adjustment approach, which consists of adjusting the vertical velocity by forcing  $w$  to be zero at the bottom and top of any column before linearly distributing the error at the top throughout the column (O'Brien 1970). Although relatively crude with respect to aforementioned adjustment techniques, this

method is fast and robust enough to achieve qualitative information on the vertical velocity field. This choice is moreover justified by the fact that this product is primarily destined for forecasters (for nowcasting) and modelers (for model verification), who most exclusively work with divergence fields. Note, however, that more efficient schemes may be used in the future depending on available computing resources.

#### 4. Examples of operational wind reconstruction

An evaluation of multiple-Doppler winds reconstructed in this operational framework is provided through analysis of observations collected during rain events that crossed the domain of analysis in 2007. A first example can be found in Bousquet et al. (2007) who investigated the structure of airflow during a long-lasting precipitation event and compared the retrieved winds against wind profiler observations. The aim of this section is to complement the aforementioned study through evaluating the reliability of the retrieved wind fields in weather situations characterized by more complex airflow structures.

##### a. Example 1: Surface occluded cyclone

The first event consists of a surface occluded cyclone, initially centered over the United Kingdom, that crossed the French territory on 27–28 May 2007. This cyclonic circulation was the center of a large-scale low pressure system that affected western Europe for a period of 1–2 days. Figure 3 depicts the surface evolution of the cyclone between 0000 and 1200 UTC 28 May 2007, which approximately corresponds to the period of available radar observations. At 0000 UTC (Fig. 3a) the cyclone was located over northern France with a central pressure of ~995 hPa. The corresponding frontal analysis shows a cold (warm) frontal zone east (north) of the cyclone center and an occluded front wrapping around the low. At 1200 UTC (Fig. 3b), the low has considerably weakened and the occluded front associated with this system has extended southward to reach the Pyrenees Mountains. The corresponding precipitation and airflow structures at 1500 m MSL deduced from the analysis of radar data collected between 0130 and 1230 UTC are shown in Fig. 4. It shows a well-organized cyclone slowly moving eastward at a speed of ~5 m s<sup>-1</sup> accompanied with weak to moderate stratiform precipitation. The strongest winds (~10 m s<sup>-1</sup>) were initially observed within an asymmetric ring collocated with the cyclone center (Figs. 4a,b). Around 0830 UTC (not shown), a well-defined rainband oriented south-to-north entered the domain of analysis. The retrieved

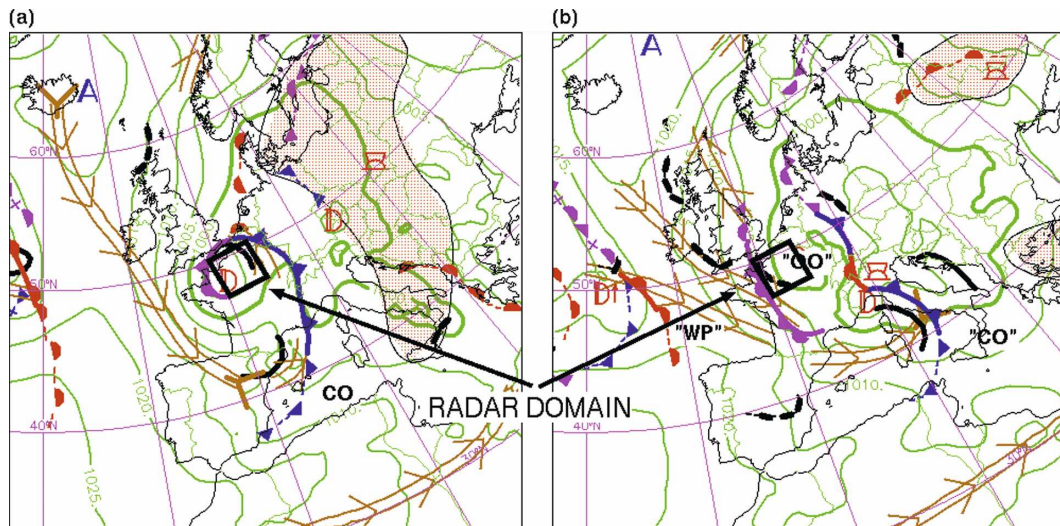


FIG. 3. Operational analyses of surface pressure and fronts on 28 May 2007 at (a) 0000 and (b) 1200 UTC. The black square indicates the location of the domain where operational wind retrieval is performed.

winds within this band were significantly stronger and could reach up to  $20 \text{ m s}^{-1}$  (Figs. 4c,d). Its location, about 140 km to the west of the cyclone center, coincides with that of the occluded front (Fig. 3b). To the best of our knowledge, this is the first time that such a phenomenon is continuously sampled by operational radars in a dual- or multiple-Doppler configuration. Exploitation of such data may be particularly interesting in terms of short-term forecasting, as it allows tracking of low pressure centers at high spatiotemporal resolution and nowcasting more accurately their future position. Such datasets could also be used in research to better understand the structure and evolution of occluded cyclones, which is still an open subject (Schultz and Mass 1993).

### b. Example 2: Squall line

To assess the quality of the wind retrieval in a more convective precipitation regime we now turn to a particularly intense and quite unusual weather phenomenon that was observed on 25 May 2007. On this day a severe squall line brought torrential rainfall in the greater Paris area and disrupted air traffic for several hours at all Paris airports. This storm initially displayed multicellular behavior, with a somewhat unorganized distribution of the cells, before evolving into a quasi-linear convective system moving northeastward toward Paris at a speed of  $\sim 15 \text{ m s}^{-1}$  (i.e.,  $9 \text{ m s}^{-1}$  to the east and  $12 \text{ m s}^{-1}$  to the north). The evolution of this convective system between 1430 and 1830 UTC is shown in Fig. 5. At 1430 UTC (Fig. 5a), the main feature in the radar domain was a northwest–southeast-oriented line

of thunderstorms characterized by reflectivity values of up to 60 dBZ. New convective cells also formed in the wake of the leading line and tried to organize into a secondary line oriented at an angle of about  $60^\circ$  with respect to the primary line. This secondary line, however, quickly dissipated as cells were advected over the stable cold pool produced by the leading convection. The flow at 1500 m, which was initially from the south (Fig. 5a), progressively turned to southwesterly (Fig. 5b) as the squall line progressed in the radar domain. Starting at 1530 UTC (not shown), a local wind maximum began to form in the stratiform region of the system. This maximum progressively increased to  $25 \text{ m s}^{-1}$  at 1830 UTC (Fig. 5c) from  $15 \text{ m s}^{-1}$  at 1630 UTC (Fig. 5b) and was located within a section of the squall line that ultimately evolved in a bow-shaped segment (Figs. 5b,c). Figure 6, which presents storm-relative horizontal winds valid at 1730 UTC and 1.5 km MSL, shows that this wind jet was the signature of a well-defined rear-to-front (RTF) inflow extending from the back of the stratiform region to the leading convective edge of the system. This inflow was restricted to the stratiform region at the rear of the bowing segment and was oriented northward (i.e., in a direction perpendicular to the apex of the bow). According to Fig. 7, which shows vertical profiles of storm-relative mean wind components within the RTF flow region, the maximum of rear inflow was observed near 1.5 km MSL with a relative peak value of  $\sim 7 \text{ m s}^{-1}$ . It was extending up to about 4 km MSL and was associated with subsiding motions. These results are in good agreement with conceptual models of bow-shaped convective systems (e.g.,

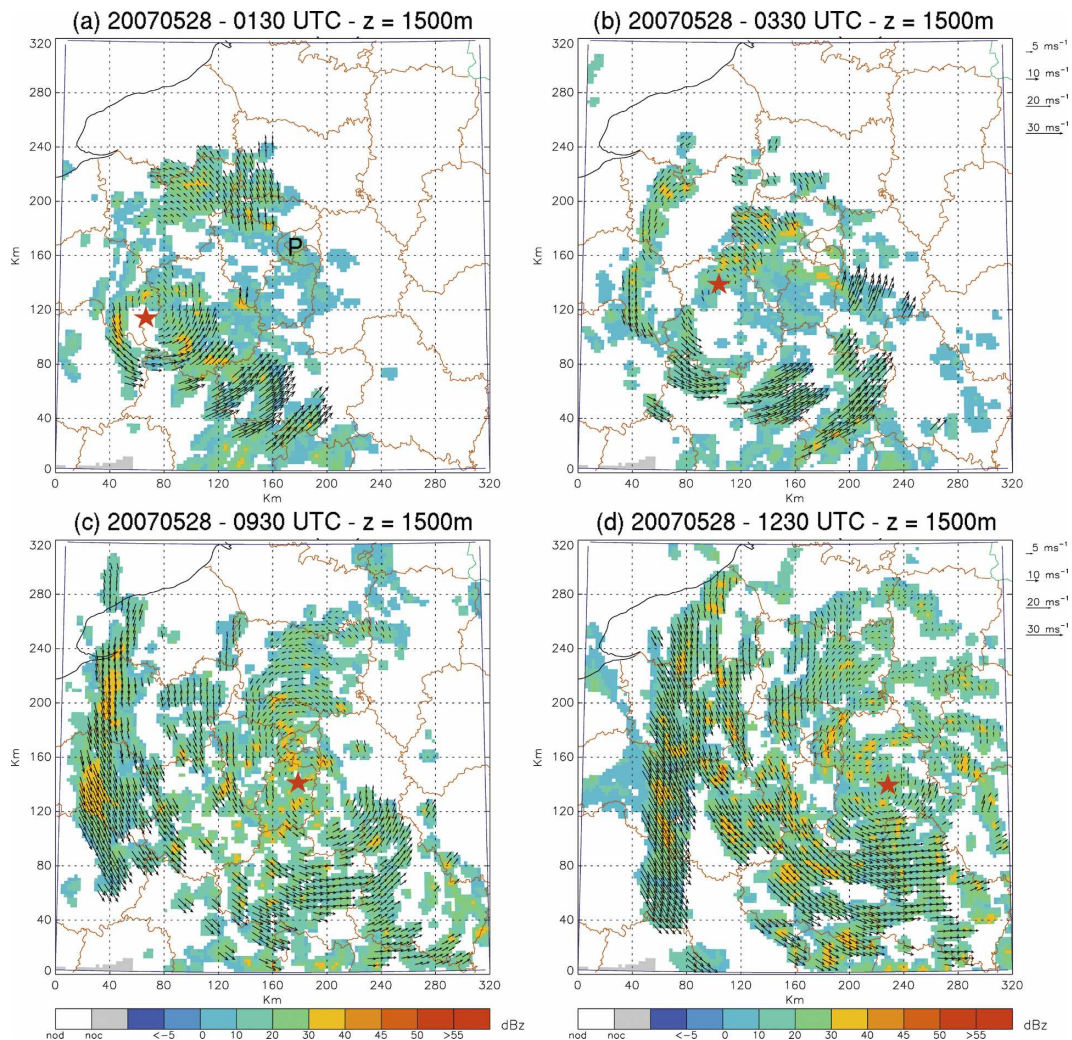


FIG. 4. Multiple-Doppler analysis of wind (vectors, key at right) at 1.5 km MSL superimposed on radar reflectivity (shaded, key at bottom) within the  $320 \times 320$  km<sup>2</sup> experimental domain shown in Fig. 1, valid at (a) 0130, (b) 0330, (c) 0930, and (d) 1230 UTC 28 May 2007. The red star indicates the approximate location of the cyclone center. In (a), label P shows Paris. One of every two vectors is plotted.

Fujita 1978; Weisman 1993; among others) as well as more recent studies inferred from radar observations collected during the Bow Echo and Mesoscale Convective Vortex Experiment (BAMEX; Davis et al. 2004). According to these studies, bow-shaped segments of convective cells generally develop 3–4 hours into the lifetime of a convective system and are always associated with a strong, generally subsiding, rear-inflow jet penetrating the leading edge of the bow. This rear-inflow jet can sometimes reach down to the surface and merge with convective outflows that develop at the rear of the convective line, resulting in substantial wind damage. In this particular case, however, it is not possible to determine if the RTF flow reached the ground because of the lack of radar overlapping below 1 km MSL.

The retrieved vertical velocity field and horizontal airflow at a height of 5 km MSL (height of the vertical velocity maximum) are shown in Figs. 5d–f. Overall there is a remarkable agreement between the retrieved vertical velocities and the structure of the reflectivity field. Maximum upward motions appear well correlated with the highest reflectivities at the system leading edge. In particular, one can note that the upward vertical velocity pattern in the convective region (including the bow-shaped segment region) almost perfectly matches that of the reflectivity cores (Fig. 5e). The strongest updrafts were observed at 1430 UTC (Fig. 5d). At 1630 UTC (Fig. 5e), updrafts start to gradually weaken at the leading edge of the line, which is in good agreement with the apparent decrease of the convective activity deduced from both reflectivity measurements

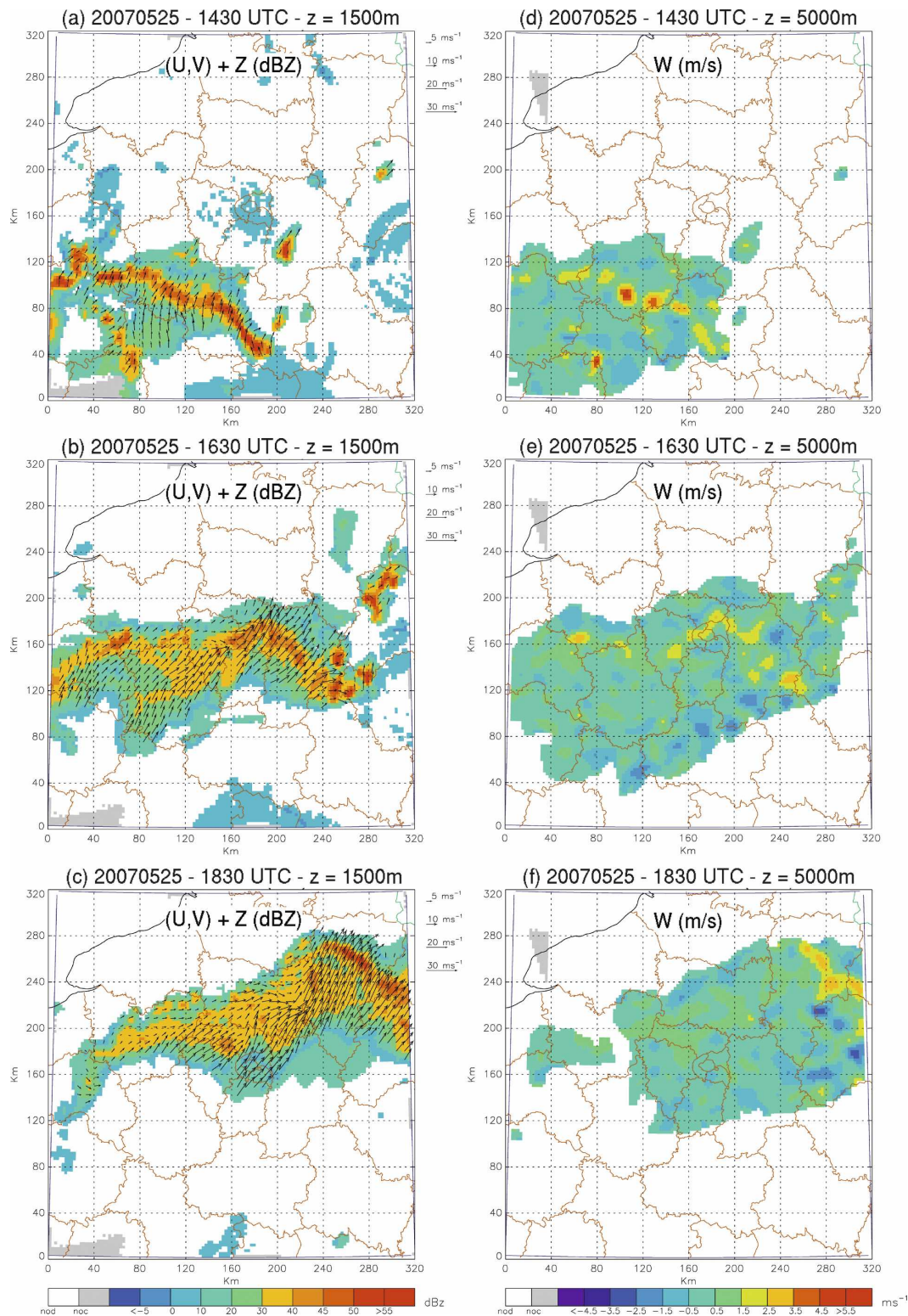


FIG. 5. Multiple-Doppler analysis of radar data at (a), (d) 1430, (b), (e) 1630, and (c), (f) 1830 UTC 25 May 2007 within the  $320 \times 320 \text{ km}^2$  experimental domain shown in Fig. 1. (a)–(c) Wind (vectors) superimposed on radar reflectivity (dBZ) at 1.5 km MSL (every third vector is plotted). (d)–(f) Vertical velocity ( $\text{m s}^{-1}$ ) at 5 km MSL.

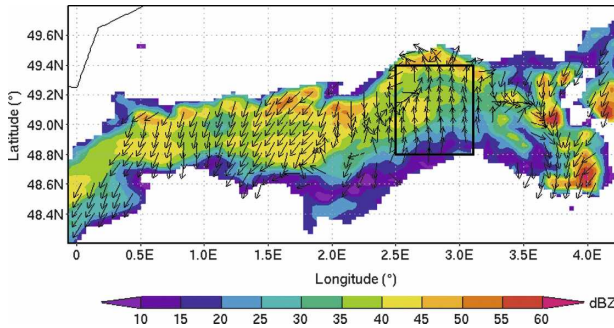


FIG. 6. Zoomed view of radar reflectivity and system relative winds for 1730 UTC 25 May 2007 at 1.5 km MSL (every third vector is plotted). The box indicates the domain where mean vertical profiles of wind components shown in Fig. 7 are computed.

and from the observation of a descending rear inflow that is often associated with decaying systems. Overall, these results suggest that retrieved vertical velocities should be exploitable from a qualitative standpoint in regions of significant vertical motions. The limitations resulting from the coarse resolution of the data, missing low-level information, and boundary conditions, however, proscribe any quantitative analysis of vertical velocity estimations.

The agreement between these results and those in-

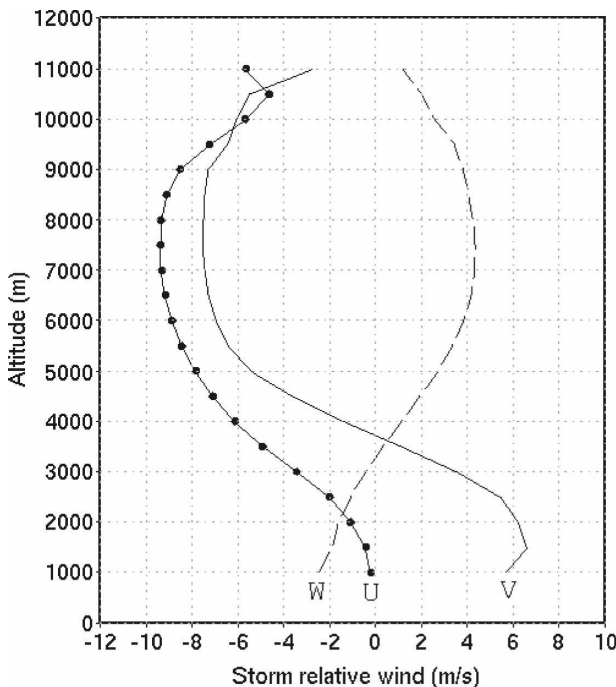


FIG. 7. Mean vertical profiles of system relative  $u$  and  $v$  wind components ( $\text{m s}^{-1}$ ) and vertical velocity  $w$  ( $\text{m s}^{-1}$ ) at 1730 UTC 25 May 2007, within the box shown in Fig. 6.

ferred from the analysis of high-resolution research data collected in recent field experiments (Wakimoto et al. 2006; Davis et al. 2004) attests to the apparent reliability of multiple-Doppler winds retrieved in the framework of the French operational radar network. Further validation is nevertheless required to routinely use this product for operational purposes such as nowcasting or model verification applications (Bousquet et al. 2008). A first assessment of this product can be found in Bousquet et al. (2007) who compared multiple-Doppler winds retrieved during a frontal precipitation event against operational wind profiler measurements over a 15-h period. This comparison was, however, only valid at the profiler site and as such, not really representative of the overall reliability of the wind retrieval. This point is of particular importance as the accuracy of retrieved winds strongly depends on geometrical considerations ensuing from the heterogeneity of the radar sampling in the domain of analysis (the profiler was, e.g., located in a region of dual- and triple-Doppler coverage where retrieved winds are theoretically less accurate than those synthesized in regions covered by four or five radars). Although the agreement between the two datasets was quite satisfactory, the authors noticed that this comparison was strongly biased when the front passed above the profiler site. This bias, which is a consequence of the poorer temporal resolution of the profiler data, illustrates quite well the challenges in validating these multiple-Doppler winds; in fact—and this is what drives the uniqueness of this product—there is currently no observation means able to provide wind measurements at the space–time resolution achieved by Doppler radars. Since the exact solution of the wind retrieval performed from real data cannot be observed in nature, the validation of these winds is thus extremely difficult. An alternative to this issue, which is often used by experimenters, consists of using simulated radar observations to evaluate more objectively the consistency of the retrieved winds. In such experiments, a reference airflow that is derived from either an analytical wind field or cloud model outputs is sampled to generate sets of simulated radar observations.

### 5. Tests with simulated radar data

#### a. Simulation procedure

In the following, numerically simulated Doppler observations are used to quantitatively assess the consistency of the reconstructed wind fields inferred from the five-radar network covering the greater Paris area. The objective of this test is not to validate the MUSCAT analysis, which has already been proven very robust,

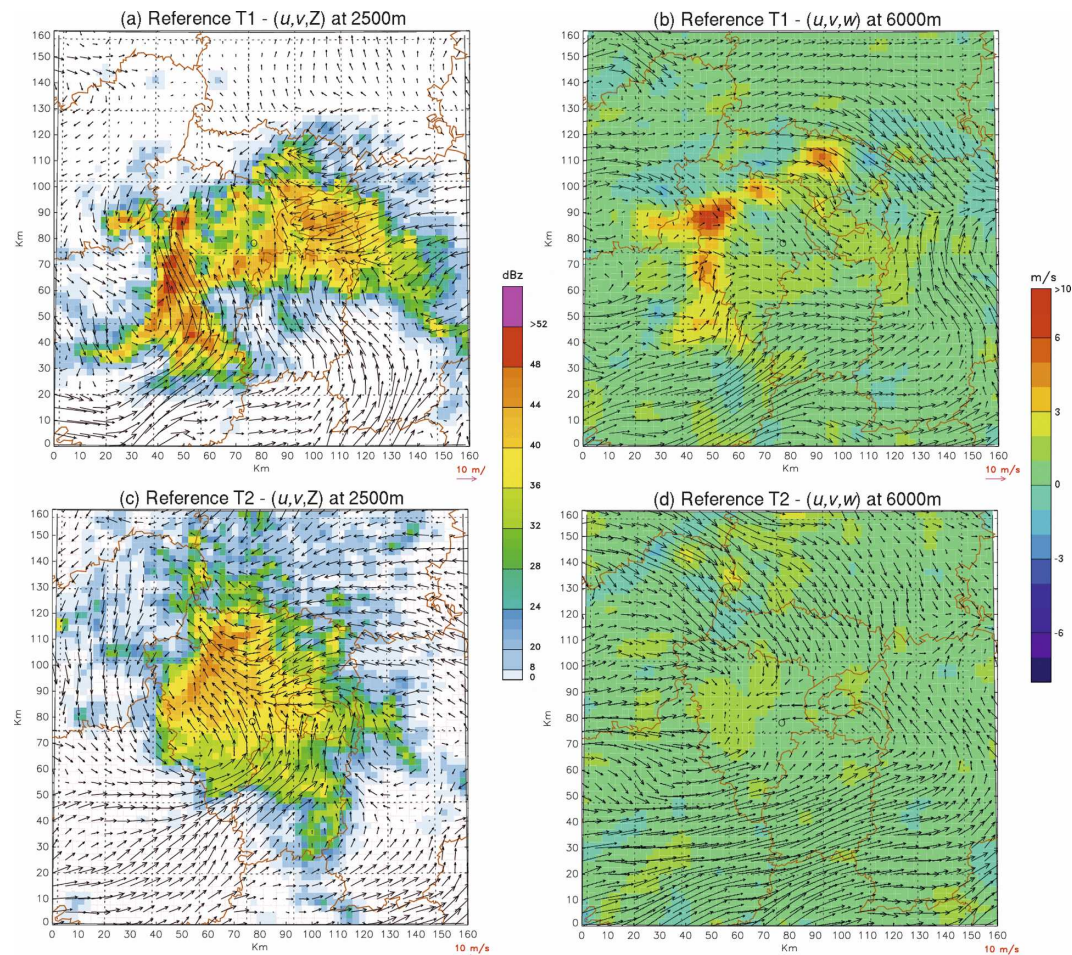


FIG. 8. Horizontal cross sections of the reference wind field at time (a), (b) T1 and (c), (d) T2. Airflow at (a), (c) 2.5 km MSL superimposed on reflectivity (dBZ) and (b), (d) 6 km MSL superimposed on vertical velocity ( $\text{m s}^{-1}$ ).

but to verify that assumptions regarding the geometry and errors made in this operational framework are acceptable. The simulated radar data are generated from a high-resolution numerical simulation of a severe storm that is used as the “true” atmosphere. This numerical simulation was performed using a nested version of the Méso-NH system, which is the nonhydrostatic mesoscale atmospheric model of the French research community (Lafore et al. 1998). The model domain used to create the simulated radar dataset is centered over Paris and measures  $160 \times 160 \times 12 \text{ km}^3$  with a grid spacing of 2.5 km in the horizontal and 300 m in the vertical (over 41 levels). Simulated radar data are generated at two distinct model output times, respectively referred to as T1 and T2 (Fig. 8). Time T1 (Figs. 8a,b) corresponds to the mature stage of the simulated system and is dominated by convective rainfall, whereas time T2 (Figs. 8c,d) corresponds to the decaying stage of the storm and is dominated by strati-

form precipitation. The detailed description of this experiment is given hereafter:

- (i) Simulated  $1\text{-km}^2$  Cartesian PPIs of reflectivity and radial velocity are constructed by sampling Méso-NH reflectivity and wind components  $u$ ,  $v$ , and  $w$  in a manner consistent with the scanning sequence of the five Doppler radars demonstrated in Table 1. A bilinear interpolation of the model grid values surrounding each observation point is used to simulate the radar sampling, and random errors with an rms value of  $1 \text{ m s}^{-1}$  are added to the simulated radial velocities to account for radar statistical error. Data associated with negative reflectivity values are also flagged out to indirectly simulate the exclusion of low signal-to-noise-ratio data. Note that potential uncertainties such as those related to velocity aliasing, beam filtering, or storm advection are not taken into account in these simulations.

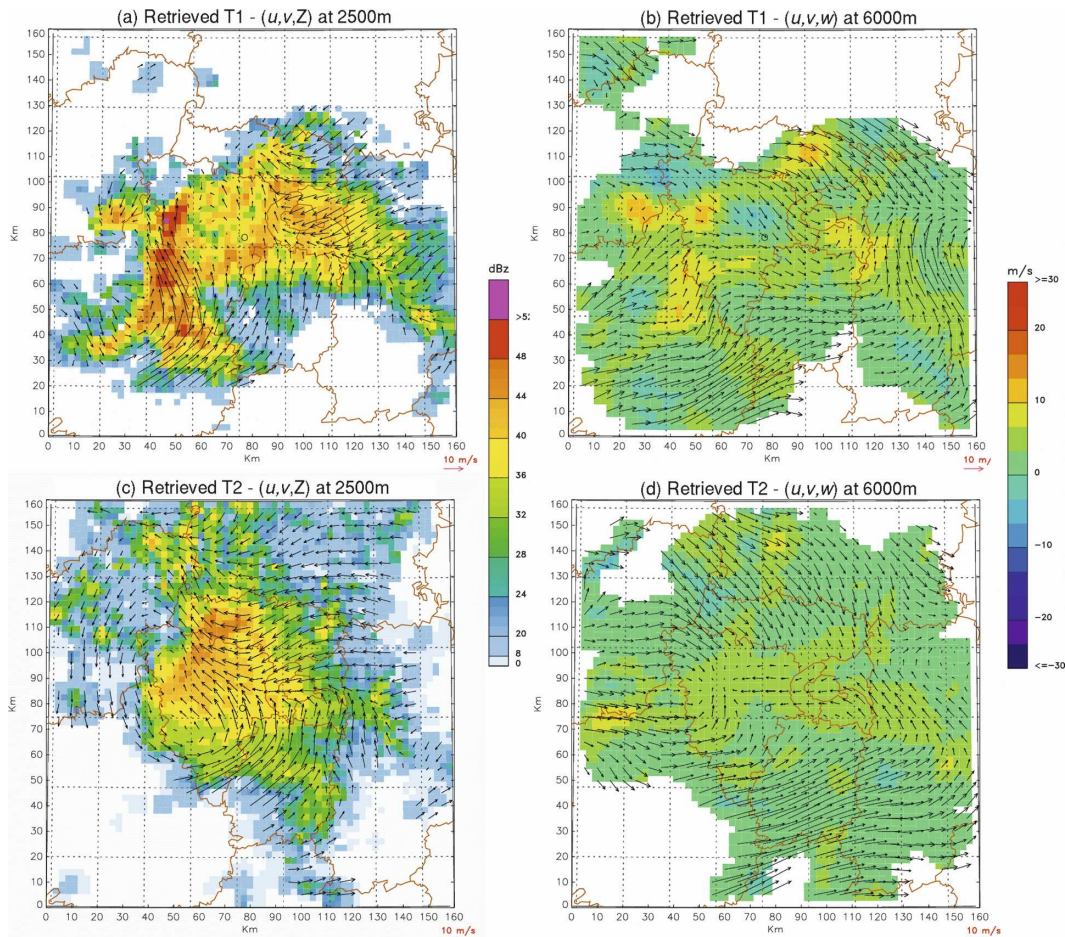


FIG. 9. As in Fig. 8, but for retrieved winds.

- (ii) The simulated PPIs are ingested in the radar processing chain presented in section 3d. The processing of simulated radar datasets is identical to that of real data (with a nil advection vector field).
- (iii) Multiple-Doppler wind fields synthesized from simulated radar datasets at times T1 and T2 (labeled RETRIEVED) are compared against original model outputs (labeled REFERENCE). The MUSCAT low-pass filter (see section 3d) being set such that the cutoff wavelength is 4 times the grid resolution ( $\sim 10$  km), model outputs are filtered at the same scale before performing any comparison with the reconstructed fields. This allows one to restrict the evaluation to only those scales that can be reproduced by the retrieval method and to mitigate scale-related representativeness errors.

*b. Results*

Retrieved winds at 2.5- and 6-km altitude corresponding to times T1 and T2 are shown in Fig. 9. With

respect to horizontal wind components, the difference between the reconstructed and the true airflow (Fig. 8) is almost imperceptible at both heights. Regions of subsiding and ascending motions also appear well positioned with respect to the reference (Fig. 8), although updrafts are generally underestimated (overestimated) in convective (stratiform) regions. Such errors are not surprising considering both the crude method used to integrate the continuity equation and missing low-level convergence ensuing from the lack of radar overlapping below 1 km MSL. The correct positioning of convective updrafts and downdrafts at time T1 (Fig. 9b), however, suggests that retrieved vertical velocities could indeed be exploitable from a qualitative standpoint in strongly convective situations. As for stratiform regions (Fig. 9d), or cases characterized by weak-to-moderate small-scale convergence, retrieved vertical velocities must be considered with caution, although the imposition of horizontal averaging could be used for extracting some information and mitigating errors resulting from

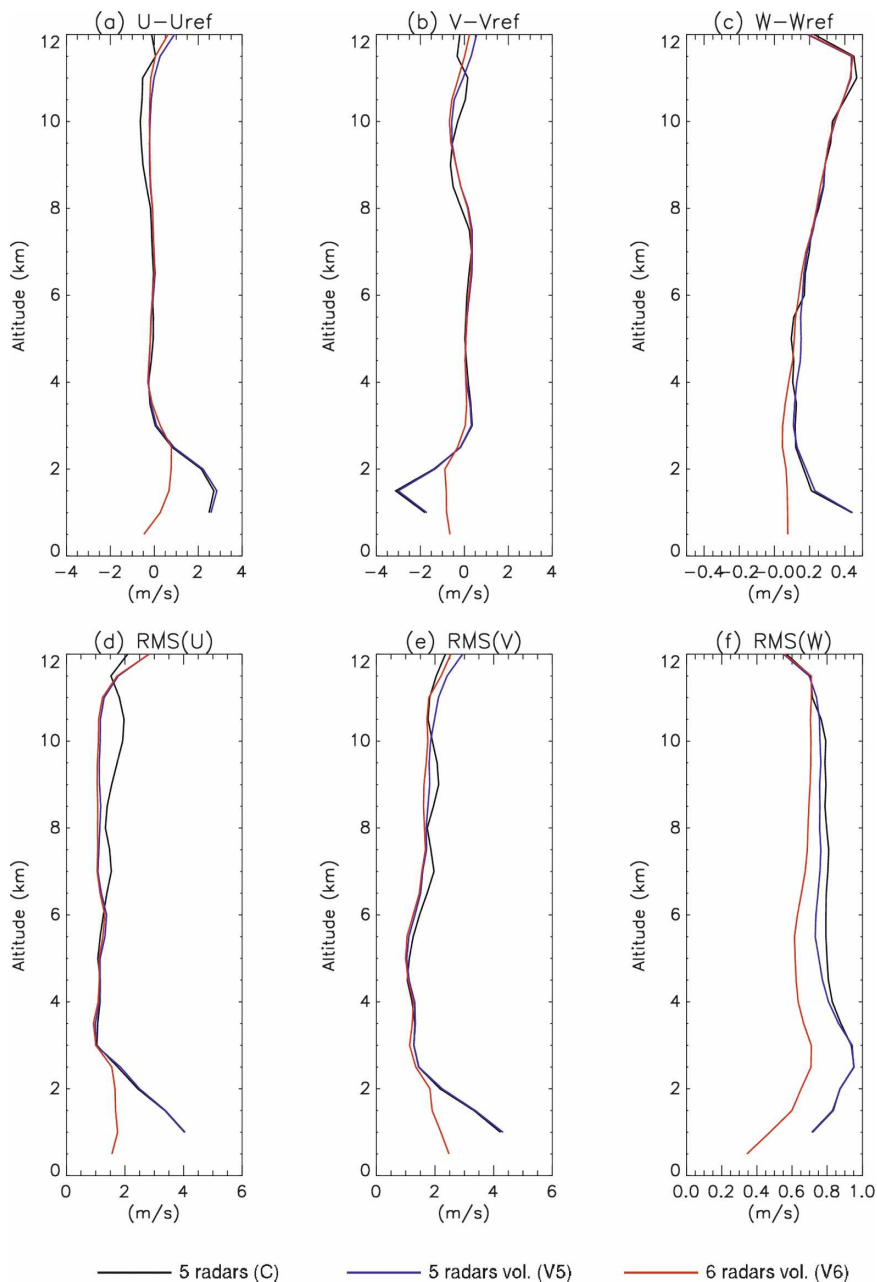


FIG. 10. Height profiles of the (a)–(c) mean and (d)–(f) standard deviation of the differences between synthesized and reference  $u$ ,  $v$ , and  $w$  components for different radar configurations (see text).

boundary conditions (Fig. 7). The vertical structure of error statistics (black curves) evaluated from the difference between retrieved and reference wind components at time T1 is shown in Fig. 10. Errors in the horizontal wind components are maximized at low levels with a bias of  $3 \text{ m s}^{-1}$  at 1.5 km MSL and standard deviations up to  $4 \text{ m s}^{-1}$  at 1 km MSL. These errors then decrease with increasing height to stabilize at

midlevels. Between 2.5 and 11 km MSL, the bias error remains below  $0.2 \text{ m s}^{-1}$  with a standard deviation less than  $1.5 \text{ m s}^{-1}$ . Error profiles at time T2 (not shown) are similar to those obtained at time T1 and also show a pronounced maximum at low levels. These error figures show that uncertainties in retrieved wind components ensuing from the limitations inherent to this particular framework, such as missing low-level in-

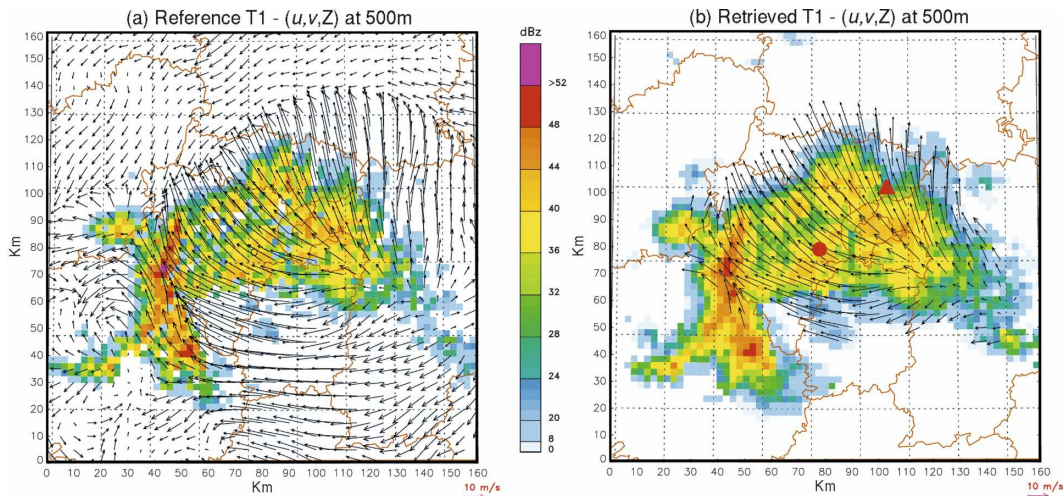


FIG. 11. Horizontal cross sections of airflow (vectors) superimposed on reflectivity (dBZ) at time T1 and 0.5 km MSL, as deduced from (a) reference and (b) V6 analysis (see text). The red triangle shows the location of the additional, virtual radar used in experiment V6. The Trappes radar is shown by a red circle.

formation or poor vertical sampling, are quite reasonable.

This simulation framework can also be used to evaluate the sensitivity of the retrieval to various parameters, as well as to test new sampling strategies or define quality indexes. With this respect, Fig. 10 also presents results of a couple of sensitivity experiments aiming to roughly evaluate the sensitivity of the retrieval to both radar density and vertical sampling so as to determine more precisely the origin of uncertainties in retrieved winds. In the first test, referred to as V5, the “volumic” scanning strategy of the Trappes radar (Table 1) is virtually applied to all other radars to achieve a denser vertical sampling of the atmosphere through scanning at higher elevations. According to associated error statistics (blue curves), the increased sampling density has little impact on the retrieval, which suggests that current radar VCPs, although quite limited, are likely sufficient to achieve a good estimation of the wind at the considered spatiotemporal resolution. In the second test, referred to as V6, the volumic scanning strategy used in experiment V5 is also applied to all radars, but an extra radar is simulated near Trappes to increase the dual-Doppler coverage near the ground. A quick evaluation of the wind retrieval in this configuration is provided in Fig. 11, which shows a side-by-side comparison of the reference and retrieved airflow at 500 m MSL. Of particular interest is the reliability of dual-Doppler winds along the radar baseline, which confirms the good performance of the retrieval method in regions of ill-conditioned analysis. The overall impact of this extra radar on the retrieval can be assessed from Fig. 10 (red curves), which shows a decrease of up to 50% in the

bias and rms errors on horizontal wind components at low levels. These results suggest that uncertainties seen immediately above the surface in the real five-radar configuration (Fig. 10, black curves) are likely a consequence of assumptions on surface winds required to initialize the wind synthesis (see section 3d). This improvement is not surprising as vertical gaps in sampled divergence (especially near the surface) are a known limitation of virtually all Doppler-derived winds. Note that the better sampling of the low-level divergence achieved through the utilization of a sixth radar also evidently improves the quality of the retrieved vertical component of the wind at all heights. This improvement is, however, relative to the five-radar configuration and is not representative of the absolute uncertainty on  $w$ .

## 6. Conclusions and perspectives

The ability to collect Doppler measurements up to long range resulting from the recent deployment of a new triple PRT scheme within the French radar network allows one to achieve extensive Doppler coverage while keeping Doppler velocity aliasing at a marginal rate. This achievement brings new perspectives in terms of exploitation of operational Doppler measurements such as the ability to routinely perform multiple-Doppler wind synthesis in a fully operational framework. In this context, an experiment has been set to produce multiple-Doppler wind fields in real time from a network of five operational radars covering the greater Paris area. This experimental setup, which has been in place since November 2006, allows producing

multiple-Doppler winds within a  $320 \times 320 \times 12 \text{ km}^3$  domain with a time resolution of 15 min and spatial resolutions of 2.5 km (horizontal) and 0.5 km (vertical).

A first evaluation of multiple-Doppler winds fields synthesized in this framework was carried out from data collected during a couple of weather situations characterized by fundamentally different airflow and precipitation regimes, that is, a surface occluded cyclone associated with moderate precipitation, and a particularly intense squall line that ultimately developed a pronounced bow-echo segment and a well-defined RTF inflow. Airflows retrieved in this operational framework are highly consistent with those documented earlier from high-resolution research radar data, which suggests that multiple-Doppler winds retrieved in this operational framework are quite reliable.

Numerically simulated Doppler radar observations have also then been relied upon to achieve a more quantitative evaluation of the retrieved airflow and to further investigate the impact of radar density and scanning strategy on the quality of reconstructed 3D winds. Results of these tests have shown that it was possible to achieve a consistent and accurate mapping of the kinematic structure of rain events despite the extensive radar baselines ( $\sim 180 \text{ km}$ ) and limited scanning strategies that characterize the French radar network in the experimental domain. The poor radar overlapping near the surface, which prevents the capture of the full low-level convergence/divergence, was nevertheless found to impact the accuracy of the retrieved horizontal circulation at the lowest levels where mean bias and rms errors could reach up to 3 and  $4 \text{ m s}^{-1}$ , respectively. These errors, however, quickly decrease with increasing height to stabilize, respectively, near 0.2 and  $1.5 \text{ m s}^{-1}$  between 2.5 and 11 km MSL, which is a remarkable result.

Although operational multiple-Doppler retrieval is currently restricted to northern France, the ongoing Dopplerization of the remaining non-Doppler ARAMIS radars should allow for the quick extension of this analysis to other parts of the French territory. With respect to this, the operational implementation, by 2010, of a nationwide, three-dimensional, wind and reflectivity composite has already been planned at Météo France and is currently under way. This product will be delivered to forecasters (mainly for visualization), to modelers for high-resolution model verification, but also to atmospheric researchers who will then benefit from unprecedented datasets for statistical or more traditional case studies. Because the typical spacing and scanning strategies of the French radars are generally comparable to those of many operational radar networks operated around the world, this achievement

could be transposed elsewhere easily and, as such, represents a remarkable opportunity to further valorize operational Doppler velocity data whose exploitation is generally limited to VAD analysis and ground filtering.

*Acknowledgments.* The authors are indebted to Laurent Périer, Jacqueline Gagneux, and Kim Do Khac (all from Météo-France) who provided essential support in software development and data management. The present work has been conducted within the scope of Flysafe (<http://www.eu-flysafe.org>), a 4-year integrated project of the Sixth Framework of the European Commission that aims to develop new airborne integrated systems for safety improvement, flight hazard protection, and all-weather operations.

## REFERENCES

- Alberoni, P. P., L. Ferraris, F. S. Marzano, S. Nanni, R. Pelosini, and F. Siccardi, 2002: The Italian radar network: Current status and future developments. *Proc. Second European Conf. on Radar Meteorology*, Delft, Netherlands, Copernicus GmbH, 339–344.
- Bousquet, O., and M. Chong, 1998: A multiple Doppler and continuity adjustment technique (MUSCAT) to recover wind components from Doppler radar measurements. *J. Atmos. Oceanic Technol.*, **15**, 343–359.
- , and —, 2000: The oceanic mesoscale convective system and associated mesovortex observed on 12 December 1992 during TOGA COARE. *Quart. J. Roy. Meteor. Soc.*, **126**, 189–212.
- , and B. F. Smull, 2006: Observed mass transports accompanying upstream orographic blocking during MAP IOP8. *Quart. J. Roy. Meteor. Soc.*, **132**, 2393–2413.
- , P. Tabary, and J. Parent du Châtelet, 2007: On the value of operationally synthesized multiple-Doppler wind fields. *Geophys. Res. Lett.*, **34**, L22813, doi:10.1029/2007GL030464.
- , T. Montmerle, and P. Tabary, 2008: Using operationally synthesized multiple-Doppler winds for high resolution horizontal wind forecast verification. *Geophys. Res. Lett.*, **35**, L10803, doi:10.1029/2008GL033975.
- Browning, K. A., and R. Wexler, 1968: The determination of kinematic properties of a wind field using Doppler radar. *J. Appl. Meteor.*, **7**, 105–113.
- , and Coauthors, 1976: Structure of an evolving hailstorm Part V: Synthesis and implications for hail growth and hail suppression. *Mon. Wea. Rev.*, **104**, 603–610.
- Chong, M., and J. Testud, 1983: Three-dimensional wind field analysis from dual-Doppler radar data. Part III: The boundary condition: An optimum determination based on a variational concept. *J. Appl. Meteor.*, **22**, 1227–1241.
- , and S. Cosma, 2000: A formulation of the continuity equation of MUSCAT for either flat or complex terrain. *J. Atmos. Oceanic Technol.*, **17**, 1556–1565.
- , and O. Bousquet, 2001: On the application of Muscat to a ground-based dual-Doppler radar system. *Meteor. Atmos. Phys.*, **78**, 133–139.
- , and Coauthors, 2000: Real-time wind synthesis from Doppler radar observations during the Mesoscale Alpine Programme. *Bull. Amer. Meteor. Soc.*, **81**, 2953–2962.

- Cressman, G. P., 1959: An operational objective analysis system. *Mon. Wea. Rev.*, **87**, 367–374.
- Davies-Jones, R. P., 1979: Dual-Doppler radar coverage area as a function of measurement accuracy and spatial resolution. *J. Appl. Meteor.*, **18**, 1229–1233.
- Davis, C., and Coauthors, 2004: The Bow Echo and MCV experiment: Observations and opportunities. *Bull. Amer. Meteor. Soc.*, **85**, 1075–1093.
- Dolan, B. A., and S. A. Rutledge, 2007: An integrated display and analysis methodology for multivariable radar data. *J. Appl. Meteor. Climatol.*, **46**, 1196–1213.
- Doviak, R. J., and D. S. Zrníc, 1993: *Doppler Radar and Weather Observations*. 2nd ed. Academic Press, 562 pp.
- Friedrich, K., and M. Hagen, 2004: On the use of advanced Doppler radar techniques to determine horizontal wind fields for operational weather surveillance. *Meteor. Appl.*, **11**, 155–171.
- Fujita, T. T., 1978: Manual of downburst identification for project NIMROD. Department of Geophysical Sciences, University of Chicago, Satellite and Mesometeorology Research Paper 156, 104 pp.
- Georgis, J.-F., F. Roux, and P. H. Hildebrand, 2000: Observation of precipitating systems over complex orography with meteorological Doppler radars: A feasibility study. *Meteor. Atmos. Phys.*, **72**, 185–202.
- Gourley, J. J., P. Tabary, and J. Parent du Chatelet, 2006: Data quality of the Météo-France C-band polarimetric radar. *J. Atmos. Oceanic Technol.*, **23**, 1340–1356.
- Holler, H., V. N. Bringi, J. Hubbert, M. Hagen, and P. F. Meischner, 1994: Life cycle and precipitation formation in a hybrid-type hailstorm revealed by polarimetric and Doppler radar measurements. *J. Atmos. Sci.*, **51**, 2500–2522.
- Houze, R. A., 1993: *Clouds Dynamics*. International Geophysics Series, Vol. 53, Academic Press, 573 pp.
- Lafore, J.-P., and Coauthors, 1998: The MESO-NH atmospheric simulation system. Part I: Adiabatic formulation and control simulations. *Ann. Geophys.*, **16**, 90–109.
- Lhermitte, R. M., and L. J. Miller, 1970: Doppler radar methodology for the observation of convective storms. Preprints, *14th Radar Meteorology Conf.*, Tucson, AZ, Amer. Meteor. Soc., 133–138.
- McLaughlin, D. J., and Coauthors, 2005: Distributed collaborative adaptive sensing (DCAS) for improved detection, understanding, and prediction of atmospheric hazards. Preprints, *Ninth Symp. on Integrated Observing and Assimilation Systems for the Atmosphere, Oceans, and Land Surface (IOAS-AOLS)*, San Diego, CA, Amer. Meteor. Soc., 11.3. [Available online at <http://ams.confex.com/ams/pdfpapers/87890.pdf>.]
- Miller, L. J., and R. G. Strauch, 1974: A dual-Doppler radar method for the determination of wind velocities within precipitating weather systems. *Remote Sens. Environ.*, **3**, 219–235.
- O'Brien, J. J., 1970: Alternative solutions to the classical vertical velocity problem. *J. Appl. Meteor.*, **9**, 197–203.
- Parent-du-Chatelet, J., M. Guimera, and P. Tabary, 2003: The PANTHERE Project of Météo-France: Extension and upgrade of the French radar network. Preprints, *31st Int. Conf. on Radar Meteorology*, Seattle, WA, Amer. Meteor. Soc., 802–804.
- Pradier, S., M. Chong, and F. Roux, 2002: Radar observations and numerical modeling of a precipitating line during MAP IOP 5. *Mon. Wea. Rev.*, **130**, 2533–2553.
- Rotunno, R., and R. Ferretti, 2003: Orographic effects on rainfall on MAP cases IOP 2b and 8. *Quart. J. Roy. Meteor. Soc.*, **129**, 373–390.
- Schultz, D. M., and C. F. Mass, 1993: The occlusion process in a midlatitude cyclone over land. *Mon. Wea. Rev.*, **121**, 918–940.
- Sugier, J., J. Parent-du-Châtelet, P. Roquain, and A. Smith, 2002: Detection and removal of clutter and anaprop in radar data using a statistical scheme based on echo fluctuation. *Proc. Second European Radar Conf.*, Delft, Netherlands, Copernicus GmbH, 17–24.
- Tabary, P., L. Perier, J. Gagneux, and J. Parent-du-Chatelet, 2005: Test of a staggered PRT scheme for the French radar network. *J. Atmos. Oceanic Technol.*, **22**, 352–364.
- , F. Guibert, L. Perier, and J. Parent-du-chatelet, 2006: An operational triple-PRT scheme for the French radar network. *J. Atmos. Oceanic Technol.*, **23**, 1645–1656.
- Torres, S. M., Y. F. Dubel, and D. S. Zrníc, 2004: Design, implementation, and demonstration of a staggered PRT algorithm for the WSR-88D. *J. Atmos. Oceanic Technol.*, **21**, 1389–1399.
- Tuttle, J. D., and G. B. Foote, 1990: Determination of boundary layer airflow from a single Doppler radar. *J. Atmos. Oceanic Technol.*, **7**, 218–232.
- Wakimoto, R. M., and R. Srivastava, Eds., 2003: *Radar and Atmospheric Science: A Collection of Essays in Honor of David Atlas*. *Meteor. Monogr.*, No. 52, Amer. Meteor. Soc., 270 pp.
- , H. V. Murphey, A. Nester, D. P. Jorgensen, and N. T. Atkins, 2006: High winds generated by bow echoes. Part I: Overview of the Omaha bow echo 5 July 2003 storm during BAMEX. *Mon. Wea. Rev.*, **134**, 2793–2812.
- Weisman, M. L., 1993: The genesis of severe, long-lived bow echoes. *J. Atmos. Sci.*, **50**, 645–670.
- Wilson, J. W., R. D. Roberts, C. Kessinger, and J. McCarthy, 1984: Microburst wind structure and evaluation of Doppler radar for airport wind shear detection. *J. Appl. Meteor.*, **23**, 898–915.
- Zrníc, D. S., 1977: Spectral moment estimates from correlated pulse pairs. *IEEE Trans. Aerosp. Electron. Syst.*, **13**, 344–354.